JOURNAL OF Applied Polymer SCIENCE

Controlling micro- and nanofibrillar morphology of polymer blends in low-speed melt spinning process. Part II: Influences of extrusion rate on morphological changes of a PLA/PVA blend through a capillary die

Nguyen Hoai An Tran,[1,2] Harald Brünig,[1] Maria Auf der Landwehr,[1] Roland Vogel,[1] Jürgen Pionteck,[1] Gert Heinrich[1,3]

[1]Leibniz-Institut für Polymerforschung Dresden e. V, Hohe Straße 6, Dresden 01069, Germany
[2]Ho Chi Minh City University of Technology, VNU-HCM, Ho Chi Minh City, Viet Nam
[3]Institut für Werkstoffwissenschaft, Technische Universität Dresden, Dresden 01062, Germany
Correspondence to: N. H. A. Tran (E-mail: tnhoaian@gmail.com) and H. Brünig (E-mail: bruenig@ipfdd.de)

ABSTRACT: The effects of the extrusion rate on the morphological changes of poly(lactic acid) (PLA)/poly(vinyl alcohol) (PVA) blend through a capillary die were investigated. In this study, the extrusion rate or mass flow rate is altered from 0.5 g min^{-1} to 2 g min^{-1} with an increment of 0.5 g min^{-1}. The PLA/PVA blend with a composition of 30/70 (wt %) exhibits a particle matrix morphology with dispersed PLA droplets within the PVA matrix. It is found that, the spherical or ellipsoidal dispersed PLA droplets are elongated and coalesced into rod-like or longer ellipsoidal droplets when they pass through the capillary die. When the extrusion rate increases, the coalescence between the large PLA droplets occurs more intense. However, the changes of the extrusion rate have no strong effect on the coalescence of small droplets having diameter less than about 150 nm. © 2016 Wiley Periodicals, Inc. J. Appl. Polym. Sci. **2016**, *133*, 44257.

KEYWORDS: extrusion rate; fibrillation process; flow rate; nanofibrillar morphology; shear flow

Received 1 June 2016; accepted 1 August 2016
DOI: 10.1002/app.44257

INTRODUCTION

The formation of micro- and nanofibrillar phase morphology of polymer blends was one of the most challenging tasks in polymer research during the last decades. Numerous studies on morphology development of polymer blends in twin-screw extruders as well as in spinneret channels, and the effects of various processing parameters on it have been published.[1–16] By contrast, few studies have tried to investigate the morphological variations of polymeric blend systems after extrusion from the spinneret orifices into fibers.[17–19] However, these investigations[17–19] were focused on investigations of the morphology of blend samples at only two positions along the spinline: blend extrudates at the die exit without stretching and the as-spun filaments on the bobbin. Recently, the study by Tran *et al.*[20] provided a new insight into the fibrillation process of PLA/PVA polymer blends, on the sample of systems in an elongational flow within the fiber formation zone in the melt spinning process. This study[20] presented the morphological development of the dispersed PLA phase via SEM images at least eight places from extrusion to take up. We found that the morphology development of PLA/PVA blends correlates well with the axial strain rate (ASR) along the spinline. However, the study was carried out only under the specific spinning condition with the take-up velocity of 50 m min^{-1} and the volumetric flow rate of 0.785 cm^3 min^{-1} (mass flow rate of 1.0 g min^{-1}). Thus, our recent study[21] attempted to investigate the morphological development of PLA/PVA blends along the spinline under other spinning conditions and to analyze the influences of the spinning conditions on the fibrillation process of polymer blends.

The fibrillation process of polymer blends in the melt spinning process on a piston-type melt spinning device is caused by the effects of the combination of the shear flow in the convergent capillary die and the elongational flow within the fiber formation zone. This article, as a second part in a three-part series of our current study, presents results on how the morphology of PLA/PVA blends changes when passing through a capillary die in a piston-type melt spinning device and the effect of extrusion rates (or flow rates) on these changes. The next article will present the morphological development of PLA/PVA blends in an elongational flow within the fiber formation zone.

The results presented here in this article are divided into two main sections starting with the morphology of PLA/PVA blend pellets obtained from the twin-screw extruder before extrusion and melt spinning. It is found that the distribution of circular equivalent diameter of the dispersed PLA droplets is very broad.

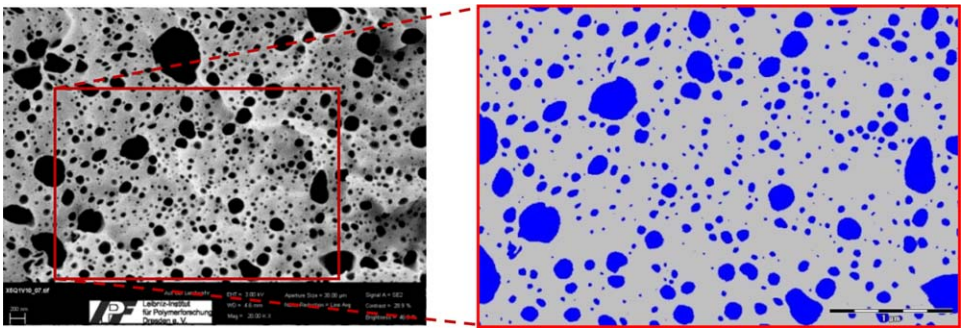

Figure 1. An original SEM image of PLA/PVA blend (a) and the image analyzed using SIA software (b). The blue domains and gray background represents the dispersed PLA phase and PVA matrix, respectively. [Color figure can be viewed in the online issue, which is available at wileyonlinelibrary.com.]

The size distribution of the dispersed PLA phase does not follow the log-normal distribution for the partial miscible PLA/PVA systems. Moreover, the experimentally determined maximum diameter of the dispersed PLA droplets is always larger than that calculated after Taylor's theory and Wu's correlation. The second section represents the morphology of PLA/PVA blend extrudates after extrusion through a convergent capillary die at various flow rates without stretching. The PVA matrix is very simple removed from the PLA/PVA blend extrudates using water only and the dispersed PLA phase can easily etched by immersing the blend into chloroform. Thus, the morphology of the dispersed PLA phase in PLA/PVA blend extrudates is easily observed in both cross-sectional and longitudinal direction of PLA/PVA blend extrudates. As a result, a whole picture of the dispersed PLA phase deformation in PLA/PVA blends with different extrusion rates can be well understood.

EXPERIMENTAL

Materials and Blend Preparations

The PLA (PLA 6202D purchased from NatureWorks LLC) and the PVA (Mowiflex TC 232 kindly donated by Kuraray Co., Ltd, Japan) were used for the melt spinning of PLA/PVA blends. The PLA/PVA blend pellets at weight ratio of 30/70 were melt compounded using a HAAKE Poly Lab OS twin screw extruder (PTW 16/25, Thermo Fisher Scientific Germany BV & Co KG, Braunschweig, Germany). The mixing temperatures at different zones along the extruder (starting from the feeding zone to the die) were 175 °C, 180 °C, 185 °C, 190 °C, 190 °C, and 180 °C. The screw speed was 100 rpm with the feeding rate of 1000 g/h. The mixed extrudates were then cut into small pellets. These pellets were melt spun as PLA/PVA-monofilament on a piston spinning device.

Melt Spinning

The melt spinning experiments were carried out using a self-constructed piston type spinning device at the Leibniz-Institut für Polymerforschung Dresden e. V. (IPF Dresden). The schematic drawing of this device can be found in Ref. 20 with the following specifications: the diameter of the cylinder was 10 mm with a length of 200 mm. The diameter and the length of the capillary hole was $D_0 = 0.6$ mm and $L = 1.2$ mm, respectively, (aspect ratio $L/D = 2$), and the entrance angle was $\alpha = 60°$. Spinning conditions for all spinning processes were fully presented in our recent work.[21] For the current study, the mass flow rate (extrusion rate) is altered from 0.5 to 2.0 g min^{-1} at an increment of 0.5 g min^{-1}.

Before melt spinning, the PLA/PVA pelletized blends were dried in a vacuum oven at 60 °C for 6 h and then filled into the cylinder under dry nitrogen. All spinning experiments were performed at 195 °C.

Morphology Characterization

Two kinds of PLA/PVA blend samples were prepared to study their morphology: the PLA/PVA blend pellets obtained from the mixing process using the twin-screw extruder; the PLA/PVA blend extrudates after extrusion through a capillary die without stretching. These blend samples were then immersed in distilled water for 24 h at room temperature (about 25 °C) or in chloroform for 8 h at 50 °C to remove the dispersed PLA phase and the PVA matrix, respectively. The remaining phase was then dried at room temperature for 24 h.

Scanning Electron Microscopy (SEM). All the dried samples were investigated using Scanning Electron Microscopy (SEM) Ultra Plus (Carl Zeiss NTS GmbH, Oberkochen, Germany). The samples were sputtered with a thin layer of 3 nm platinum to hinder electrostatic charging.

Images Analysis. SEM images of PLA/PVA blends were evaluated using Scandium Image Analysis Software (SIA) (Olympus soft imaging solutions GmbH, Münster, Germany). This program automatically detects the dispersed PLA phase (as black holes after PLA extraction) (Figure 1). The size and shape of dispersed PLA domains such as perimeter, circular equivalent diameter (CED), aspect ratio, circularity, etc. can be easily obtained using this program. However, the program can only be helpful if the holes and background of the images have sufficient contrast. Therefore, in this study, the shape and size of the dispersed PLA phase were measured both manually and automatically with the SIA program. The CED d_{CED}, the number-average CED $\bar{d}_{CED}$, and circularity/form factor were used as characteristic morphological parameters to describe the dispersed PLA phase particles. These parameters are defined as follows (Figure 2)[22,23]:

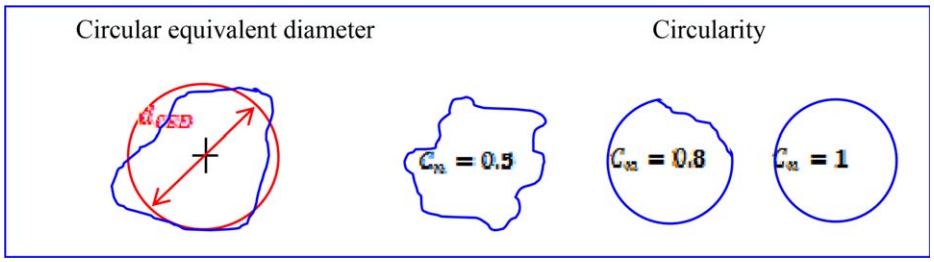

Figure 2. Illustrating of circular equivalent diameter (left) and circularity of a two-dimensional particles (right). [Color figure can be viewed in the online issue, which is available at wileyonlinelibrary.com.]

Circular equivalent diameter (CED) or equivalent area diameter, d_{CED}: Diameter of a circle having the same area as the surface of the particle. It can be calculated using the eq. (1)

$$d_{CED}=\sqrt{\frac{4A}{\pi}} \quad (1)$$

where A is the area of the particle

Number-averaged CED $\bar{d}_{CED}$ was defined as follows:

$$\bar{d}_{CED}=\frac{\sum n_i d_{CEDi}}{\sum n_i} \quad (2)$$

where n_i is the number of dispersed phase domains with d_{CED}

Circularity or form factor, C_n: There are several definitions of the circularity.[24] In this study, the circularity is evaluated according Cox's equation [eq. (3)], where P is perimeter. It is the ratio of the area of the particle to the area of a circle with the same perimeter. $C_n=1$ indicates a perfect circle and $C_n \rightarrow 0$ points out to increasingly elongated polygon.

$$C_n=\frac{4\pi A}{P^2} \quad (3)$$

The size/diameter of the dispersed PLA phase in PLA/PVA blend extrudates after removing the PVA matrix was also manually measured using SIA. For the ellipsoidal droplets, the maximum sizes are selected to determine their diameters (Figure 3).

RESULTS AND DISCUSSION

Morphology of PLA/PVA Blend Granules

Figure 4 shows the SEM images of the PLA/PVA 30/70 blend pellets obtained from the twin-screw extruder before extrusion and melt spinning on the piston melt spinning device. Figure 5 presents frequency-distribution histograms of about 174,000 dispersed PLA droplets in the fractured area of 114.7 × 74.1 μm^2 of a SEM image. For completely immiscible polymer blends, the size of the dispersed phase exhibits often log-normal behavior.[25–28] However, for the partial miscible PLA/PVA systems with the presence of potential H-bonding,[29] the fitting of the log-normal distribution seems to be not suitable, because the cumulative PLA droplet size distributions could not be fitted to a reference line as shown in Figure 6(c). This observation agrees well with that reported by Harrats,[25] who found that the log-normal distribution does not apply for the partial miscible polymer blends.

It is seen from Figure 5 that the distribution of circular equivalent diameters (CEDs) of PLA droplets is very broad and the CEDs range from about 0.03 to 12.1 μm with an average number CED of 0.09 μm. The distribution of CED of PLA droplets can be roughly divided in two groups, in which CEDs are smaller and bigger than 0.5 μm. There are 98.6% the number of droplets having diameter up to 0.5 μm [Figure 6(a,c)], only 1.4% having diameter larger than 0.5 μm (including 1% droplets having diameter within 0.5 to 1 μm, and a few droplets about 0.4% have diameter larger than 1 μm) [Figure 6(b,c)]. Furthermore, while the droplets having CEDs $\leq$ 0.5 μm are almost perfectly spherical, the droplets having CEDs $>$ 0.5 μm are not a spherical but rather an ellipsoidal, cylindrical or elongated shape [Figure 4(a,b)]. The calculated average circularity C_n of droplets with CEDs $<$ 0.5 μm and CEDs $>$0.5 μm is about 0.95 and 0.78, respectively. An explanation might be that the small droplets are deformed more difficult than the large droplets under shear flow during mixing in twin-screw extruder. The large droplets tend to deform and then break up into smaller ones. It is worth pointing out here that although there are few large droplets, the volume of these droplets is considerable attention. The volume contribution may be more informative than the CED distribution. But, in the present study, the volume distribution could not be determined due to the ellipsoidal, cylindrical, or elongated shape of the PLA droplets.

In principle, the largest diameter of PLA droplet D_{max} may exist under simple shear flow in Newtonian and polymer blend systems can be estimated using Taylor's theory[30] [eq. (4)] and Wu's correlation[31] [eq. (5)], respectively:

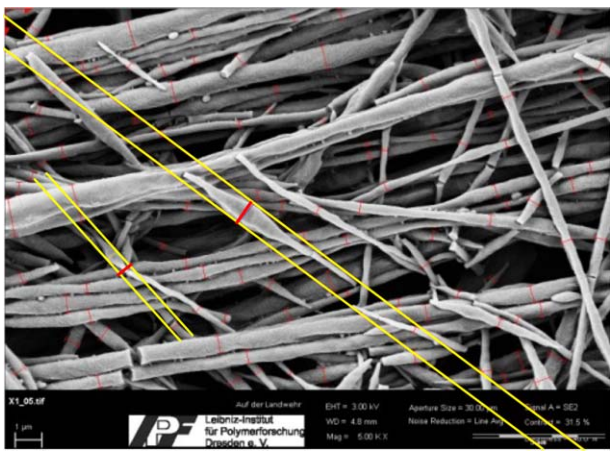

Figure 3. An example of the measurement of dispersed PLA phase determined using SIA. [Color figure can be viewed in the online issue, which is available at wileyonlinelibrary.com.]

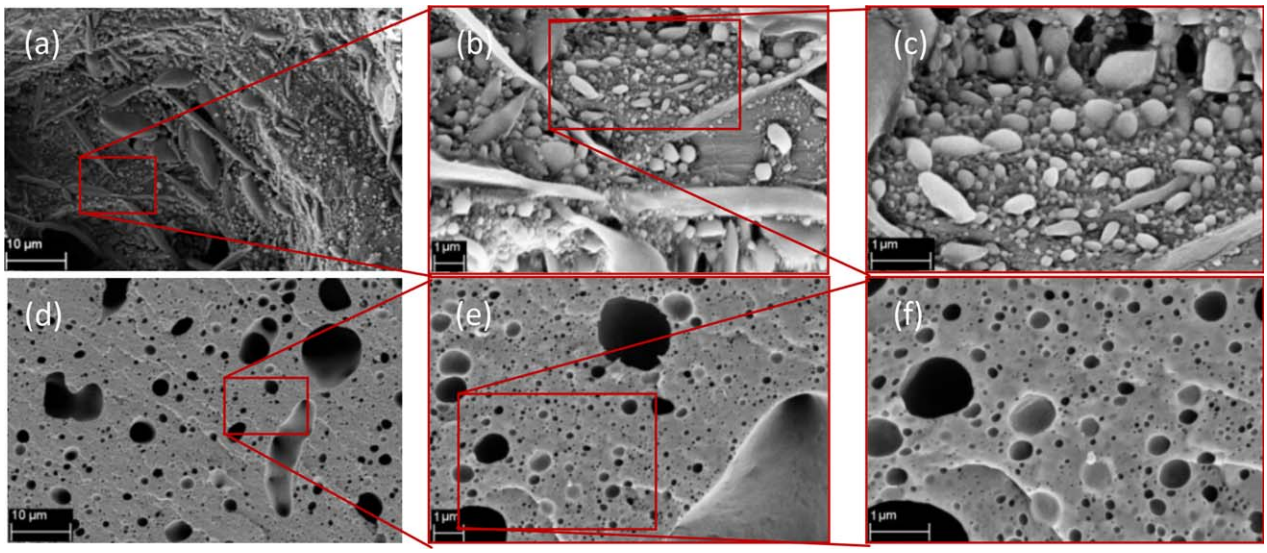

Figure 4. SEM images of the PLA/PVA 30/70 blend pellets after removing the PVA matrix (a–c) and etching the PLA dispersed phase (d–f) with scale bars for the left, middle, and right column are 10, 1, and 1 μm, respectively. [Color figure can be viewed in the online issue, which is available at wileyonlinelibrary.com.]

$$D_{\text{Taylor}} = \frac{4\Gamma(\eta_r + 1)}{\dot{\gamma}\eta_m\left(\frac{19}{4}\eta_r + 4\right)} \quad \text{for } \eta_r < 2.5 \tag{4}$$

$$D_{\text{Wu}} = \frac{4\Gamma\eta_r^{-0.84}}{\dot{\gamma}\eta_m} \quad \text{for } \eta_r < 1.0 \tag{5}$$

where $\Gamma = 1.6$ mN m^{-1} is the interfacial tension. The calculation of the interfacial tension between PLA and PVA can be seen in Appendix, $\eta_r = \eta_d/\eta_m$ is the viscosity ratio between the dispersed phase viscosity η_d and the matrix viscosity η_m, and $\dot{\gamma}$ is the shear rate. η_r and η_m are obtained using oscillatory rheometer.[32] It is worth noting here that the viscosities η_r and η_m depend on shear rate. Shear rate $\dot{\gamma}$ during mixing in twin-screw extruder at the screw speed of 100 rpm is discussed as follows.

In twin-screw extruder, polymers are subjected to complex shear and elongational deformations, and complex temperature profiles along the various zones of the extruder barrel. Therefore, it is difficult to characterize the type and magnitude of the strain rate in an extruder by a single number. However, an "average shear rate" and "effective shear rate" may be used to approximately determine shear rate.[31] Suparno *et al.*[33] has theoretically predicted that the average shear rate linearly increases with the increase of screw speed and he found that the average shear rate is about 50 s^{-1} at the screw speed of 100 rpm. Wu[31] and Burkhardt[34] pointed out that the effective shear rate G in s^{-1} is almost equal to the crew speed n in rpm: $G \cong n$. In the present study, a crew speed of 100 rpm was used. Thus, it is assumed that during mixing of the PLA/PVA blends with the screw speed of 100 rpm, the effective shear rate is 100 s^{-1} and the shear rate may vary from a few rad s^{-1} to 100 rad s^{-1} within mixing zone in twin-screw extruder.

Figure 7 gives the comparison of the measured maximum diameter $D_{\text{Measurement}}$ with the calculated maximum diameter of PLA droplets after Taylor's theory D_{Taylor} [eq. (4)] and Wu's

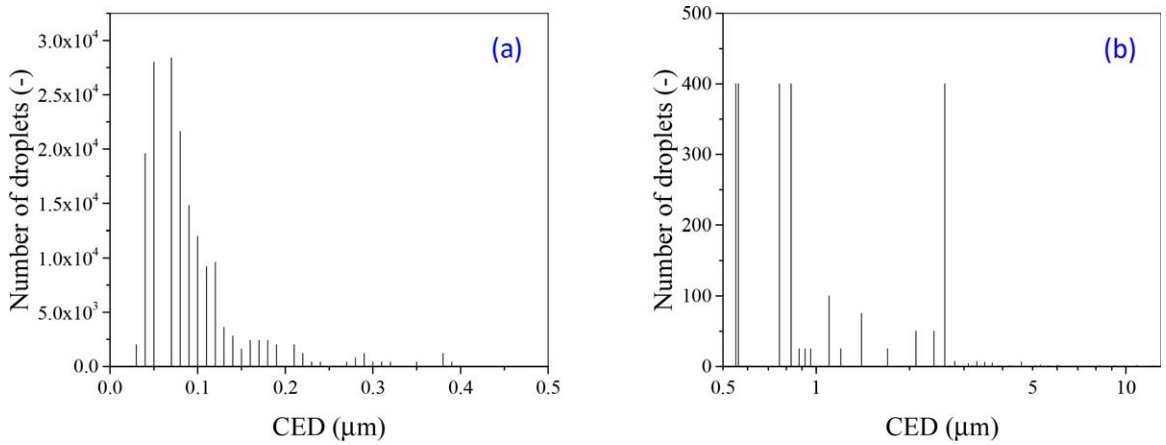

Figure 5. Frequency-distribution histograms versus circular equivalent diameter (CED) over the range of CED up to 0.5 μm (a) and CED from 0.5 to 13 μm (b). [Color figure can be viewed in the online issue, which is available at wileyonlinelibrary.com.]

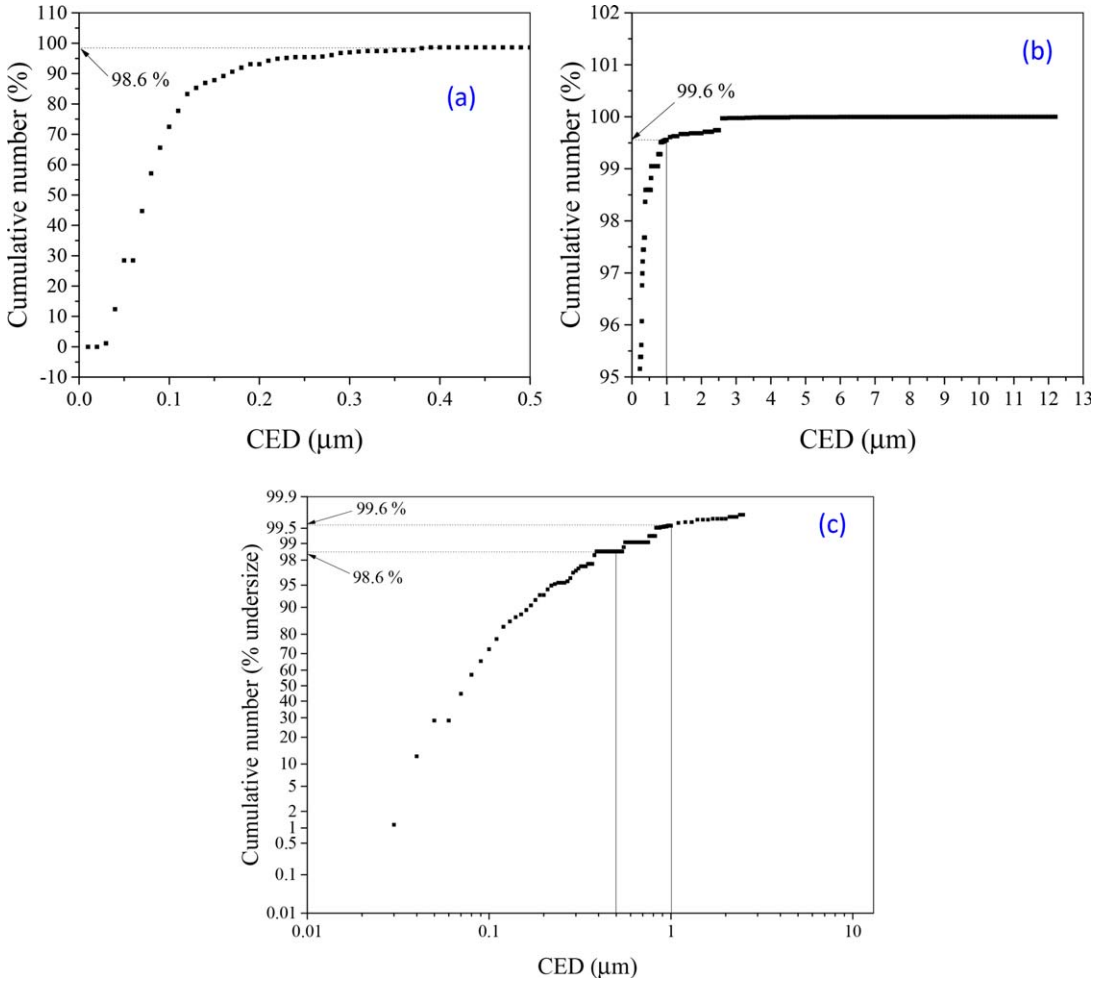

Figure 6. Cumulative number percentage versus CED (a,b) and log-normal distributions (c). [Color figure can be viewed in the online issue, which is available at wileyonlinelibrary.com.]

correlation D_{Wu} [eq. (5)] within shear rate range from 0.01 to 100 rad s^{-1}. It is seen that the $D_{Measurement}$ is always larger than the D_{Taylor}. It has almost the same value of about 12 μm with D_{Wu} at the shear rate of 1 rad s^{-1} [Figure 7(b)]. As discussed above, the effective shear rate for the screw speed of 100 rpm is definitely larger than 1 s^{-1}. Thus, it can be clearly seen from

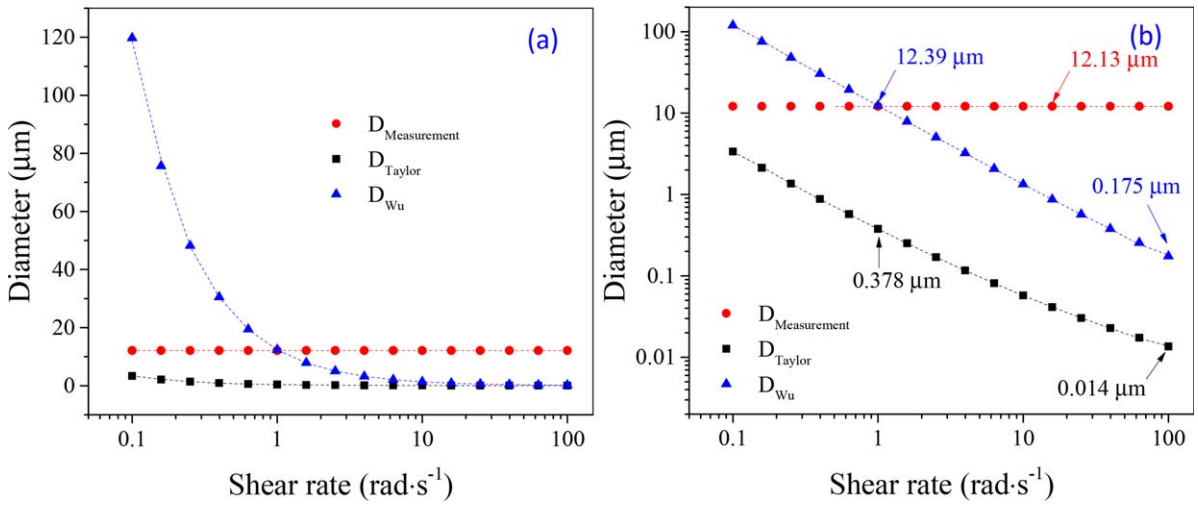

Figure 7. Comparison of the maximum diameter of PLA droplet versus shear rate range: (a) linear scale and (b) logarithmic scale for the *y*-axis (vertical axis). [Color figure can be viewed in the online issue, which is available at wileyonlinelibrary.com.]

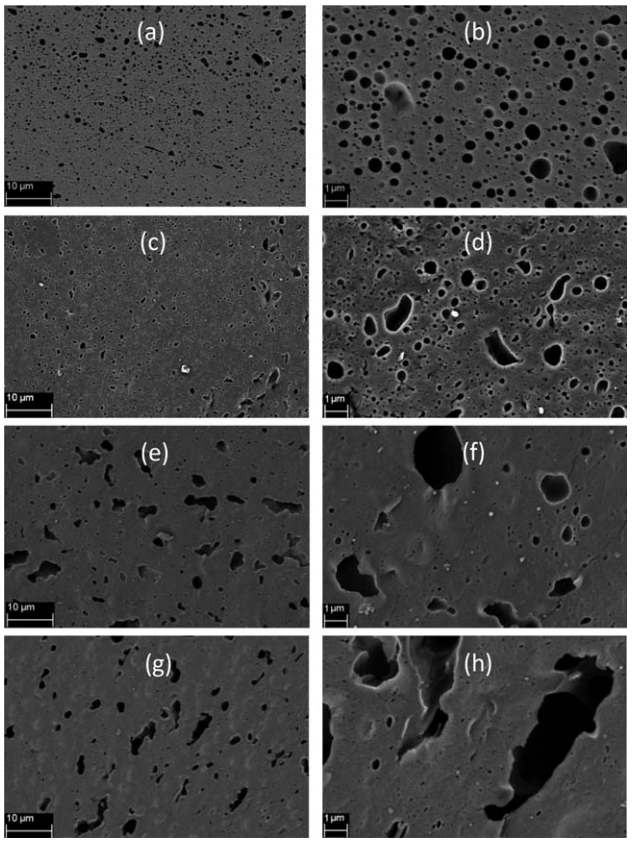

Figure 8. Morphology of the cross-sectional surfaces of PLA/PVA blend extrudates after etching the dispersed PLA phase for the various mass flow rates of 0.5 (a,b), 1.0 (c,d), 1.5 (e,f), and 2.0 g min^{-1} (g,h). The scale bars for the left to right column are 10 and 1 μm, respectively.

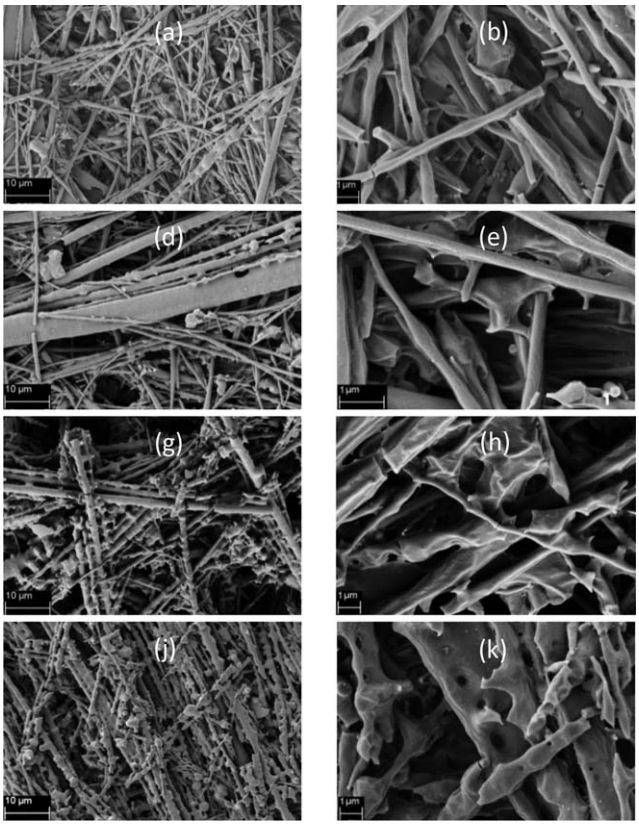

Figure 9. Morphology of the dispersed PLA phase after removing the PVA matrix for the various mass flow rates of 0.5 (a,b), 1.0 (c,d), 1.5 (e,f), and 2.0 g min^{-1} (g,h). The scale bars for the left to right column are 10 and 1 μm, respectively.

Figure 7(b) that the $D_{Measurement}$ is also always larger than the D_{Wu}. It is worth pointing out here that the Taylor's theory was employed for Newtonian liquid mixtures independent on the blend ratio and Wu's correlation was used for two specific blend systems: ethylene-polypropylene rubbers as a dispersed phase in PA66 and PET matrix with the concentration of the dispersed phase of 15%. In the present study, the used concentration of the dispersed phase is 30% much higher than that used in Wu's correlation. It is well known that coalescence can occur at values of dispersed phase as low as 1% and it increases with increasing dispersed phase content.[35] Due to the coalescence of the high PLA content (30%) in PLA/PVA blend, the measured maximum diameter is larger than the calculated maximum diameter after the Wu's correlation ($D_{Measurement} > D_{Wu}$).

Morphology of PLA/PVA Blend Extrudates

Figure 8 presents the SEM images of the cross-sectional surfaces of PLA/PVA blend extrudates after etching the dispersed PLA phase. Figure 9 shows the SEM images of dispersed PLA phase after removing the PVA matrix from the PLA/PVA blend extrudates without stretching for various mass flow rates or extrusion rates. It is seen that as the mass flow rate increases, the maximum circular equivalent diameter (CED) of PLA droplet increases (Figures 8−10). However, the number of PLA droplets [Figure 11(a)] and the number-averaged CED $\bar{d}_{CED}$ decrease (Figure 10) with the increase of the mass flow rate. These results can be explained due to the coalescence process during extrusion through a convergent capillary die as follows.

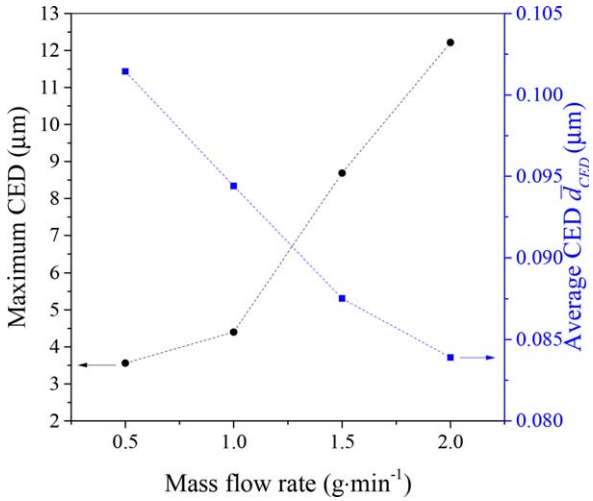

Figure 10. Maximum and number average CED $\bar{d}_{CED}$ versus mass flow rate for the cross-section of PLA/PVA blend extrudates after etching the dispersed PLA phase (measured from Figure 8). [Color figure can be viewed in the online issue, which is available at wileyonlinelibrary.com.]

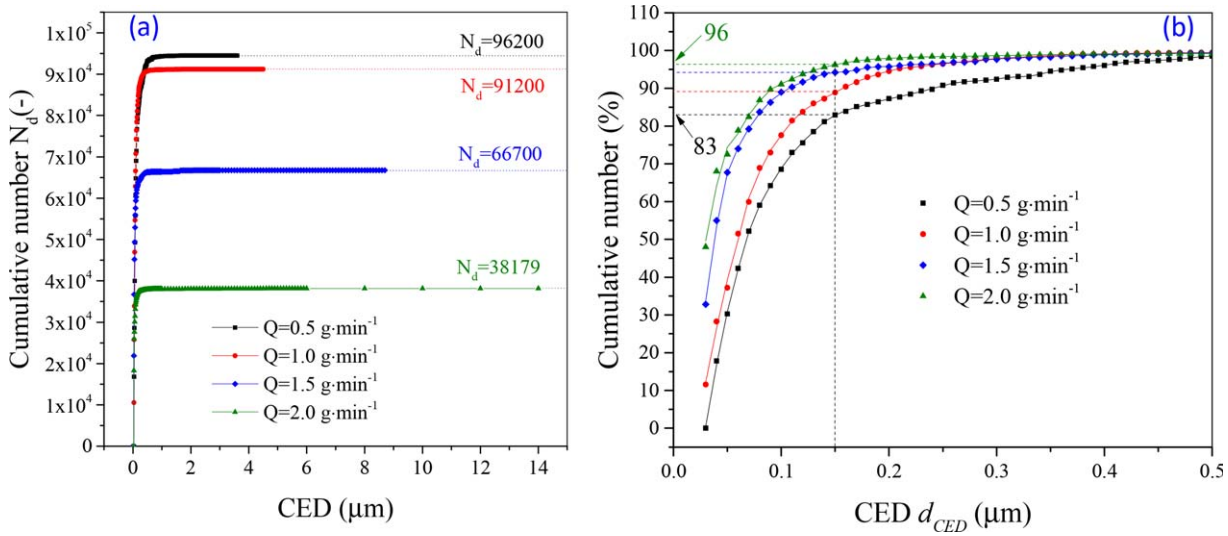

Figure 11. Cumulative number versus CED (a), Cumulative number percentage versus CED (b). [Color figure can be viewed in the online issue, which is available at wileyonlinelibrary.com.]

When the PLA/PVA blends are forced to flow through a capillary die in piston-type melt spinning device [Figure 12(b)], they are subjected to only normal stress (force acting perpendicular to the surface) in the zone A, but in the entry zone B both normal and shear stress (force acting parallel to the surface) are acting on the PLA/PVA blends. These normal and shear stresses in the zone B affect the deformation process of the PLA droplets. As a result, the sphere droplets are rotated, elongated, and coalesced into rod-like or ellipsoid shape. Then the deformed droplets pass through the die in the zone C and may keep their shapes as they immediately leave the die exit, because the used *L*/*D* ratio of 2 of capillary die is too small and the residence time of polymer blends in the die is in fact too short to deform the droplets further. The calculated residence times are only about 0.05 and 0.01 second for the mass flow rate of 0.5 and 2.0 g min^{-1}, respectively.

As the mass flow rate or extrusion rate increases, the normal and shear stresses acting on the PLA droplets in the entry zone B increases due to the increase of the pressure from 22.9 to 46.5 bar (1 bar = 100 kPa) for mass flow rate from 0.5 to 2.0 g min^{-1}, respectively [Figure 12(a)]. Generally, according to eq. (4) for Newtonian system and eq. (5) for the specific polymer blends with the dispersed phase content of 15%, the increase of shear stresses or shear rates can decrease the size of droplets. This phenomenon is often, but not always true at least in this study. For instance, the maximum CED of PLA droplets almost linearly increases from 3.6 to 12.2 μm with the increase of the mass flow rate from 0.5 to 2.0 g min^{-1} (Figure 10). This unexpected phenomenon may happen in this PLA/PVA 30/70 blends due to the coalescent process of the high content of the dispersed PLA phase and the viscoelastic behaviors of materials, which are well demonstrated by Sundararaj

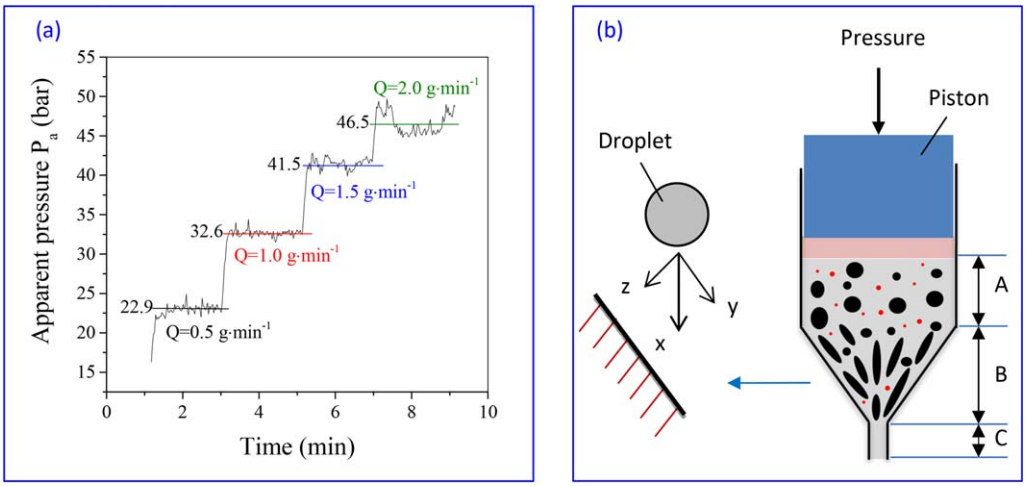

Figure 12. Measured pressure for various mass flow rates (a) and total pressure acting on the polymer blends in a convergent capillary die (b): the red color droplets represent the very small droplets. There has been almost no coalescence among these small droplets when they passing through a convergent capillary die. [Color figure can be viewed in the online issue, which is available at wileyonlinelibrary.com.]

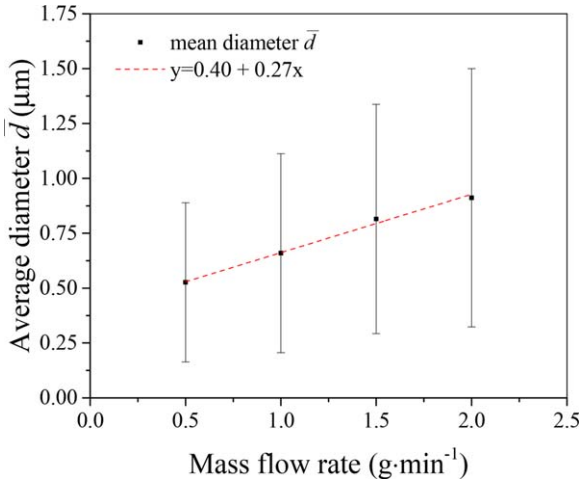

Figure 13. Mean diameters $\bar{d}$ with deviations of the dispersed PLA phase from PLA/PVA blend extrudates after removing the PVA matrix for various mass flow rates (measured from Figure 9). [Color figure can be viewed in the online issue, which is available at wileyonlinelibrary.com.]

and Macosko.[36] This anomaly has also been reported by Roland and Böhm[37], and other researchers.[38,39] Roland and Böhm[37] concluded that the droplets have higher velocities at higher shear rates and therefore the coalescence probability can increase. According to Allan and Mason,[40] the flow-induced coalescent mechanism of two Newtonian liquid drops can be represented as follows: a pair of particles come close to each other and rotate in the shear field, the thickness of matrix film between the particles then decreases until the interface ruptures, and coalescence occurs.

The coalescence increases with the increase of flow rates. This explains why the number of droplets decreases as flow rate increases [Figure 11(a)]. It is also seen from Figure 10 that the average CED slightly decreases with the increase of mass flow rates. If the average CED of PLA droplets decreases, the mean length of PLA droplets must increase, because the dispersed PLA phase is under constant volume during extrusion. This result confirmed once again that the coalescence becomes more efficient at higher mass flow rates.

Comparing Figures 8 and 9, it is interesting to note that the PLA droplets having CED less than about 0.15 μm have not been found in the remaining PLA phase after removing the PVA matrix (Figure 9) but they can be seen a lot in Figure 8 and they occupy about 83, 89, 94, and 96% of total PLA droplets for mass flow rate of 0.5, 1.0, 1.5, and 2.0 g min^{-1}, respectively [Figure 11(b)]. This observation allows one to assume that the PLA droplets having CED less than about 150 nm are removed together with the PVA matrix. Therefore, it can be predicted that there has been almost no coalescence among these small droplets [the red color droplets in Figure 12(b)] when they passing through the capillary die.

The mean diameters of the dispersed PLA phase $(\bar{d})$ from PLA/PVA blend extrudates after removing the PVA matrix for various mass flow rates (Figure 13) are much larger (about 10 times) to that of the dispersed PLA phase in cross-sectional PLA/PVA blend extrudates after etching the PLA phase ($\bar{d}_{CED}$) (Figure 10) ($\bar{d} \approx 10\ \bar{d}_{CED}$). Furthermore, the mean diameter $\bar{d}$ increases with the increase of mass flow rate (Figure 13). This tendency is opposite to the result that was found in the cross sectional PLA/PVA blend extrudates after etching the PLA phase, that is the $\bar{d}_{CED}$ decreases with the increase of mass flow rates (Figure 10). This phenomenon may be caused by the two following reasons: (1) as the mass flow rate increases, the normal and shear force are acting on the droplets increases. It makes the small droplets easier to combine together to form large ones. After the Taylor's theory for the droplet deformation, the large droplets are then deformed into ellipsoidal shapes easier than the small ones.[41] (2) When an ellipsoid is formed, the experimental values obtained by measurement the PLA ellipsoidal droplets on the fractured or cut surfaces may be imprecise, because one does not know where the ellipsoidal droplets are exactly cut and then measured. An ellipsoidal droplet can be cut through its center or any other positions (Figure 14). This may explain the reason why the $\bar{d}_{CED}$ of droplets with the higher mass flow rates is slight smaller than that with the lower mass flow rates.

CONCLUSIONS

By varying the extrusion rate or flow rate, the morphology of the dispersed PLA phase in PLA/PVA blend extrudates can be controlled. While the maximum circular equivalent diameter (CED) of PLA droplets increases, the number of PLA droplets and the number-averaged CED decrease with increase of the extrusion rate. This unexpected phenomenon occurs due to the coalescence of the high content of the dispersed PLA phase. Furthermore, at higher extrusion rate, the droplets have higher

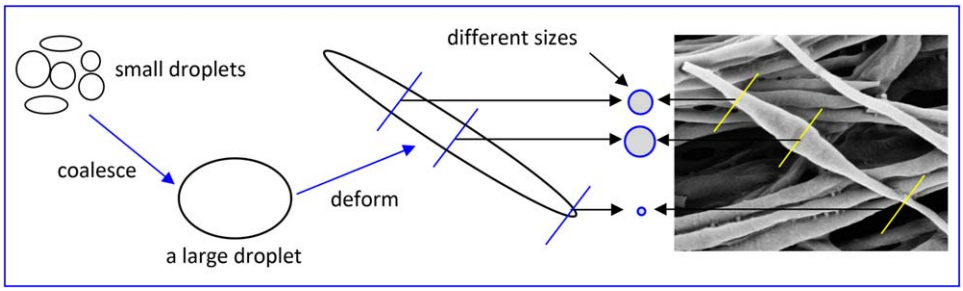

Figure 14. Schematic presentation of coalescence and deformation of droplets and different possible diameters of an ellipsoidal PLA droplet in PLA/PVA blend extrudates. [Color figure can be viewed in the online issue, which is available at wileyonlinelibrary.com.]

velocities under the effect of the increase of stresses and therefore the coalescence can happen more frequently than that at lower extrusion rate.

Owing to the morphology investigation in both cross sectional and longitudinal direction of PLA/PVA blend extrudates, the changes in morphology of PLA/PVA blends can be well understood. It was found that the large PLA droplets tend to deform and coalesce easier than the smaller ones. The coalescence between the large PLA droplets becomes more efficient as the flow rate increases. However, the increase of the flow rate did not have a strong impact on the deformation and coalescence of the very small (ca. 150 nm) PLA droplets. There is almost no coalescence among these small droplets when they were extruded through the convergent capillary die.

ACKNOWLEDGMENTS

Authors thank the financial support of the German Research Foundation within the research project "Entwicklung eines neuartigen Filamentgarnes" (BR 1886-/6-1). Authors are very grateful to Mr. Norbert Smolka and Mr. Mathias Häschel for their kind assistance with numerous melt spinning experiments. N.H.A. gratefully thanks the Vietnamese Ministry of Education and Training for a doctoral scholarship.

APPENDIX

The interfacial tension $\Gamma_{\Gamma_{PLA,\ PVA}}$ between poly(lactic acid) (PLA) and poly(vinyl alcohol) (PVA) in this study was estimated by theoretical calculation using the following eq. (A.1) [42]

$$\Gamma_{PLA,\ PVA} = \Gamma_{PLA} + \Gamma_{PVAL} - 2\phi\sqrt{\Gamma_{PLA}\Gamma_{PVA}} \qquad (A.1)$$

where Γ_{PLA} and Γ_{PVA} are the surface tension of PLA and PVA, respectively. The interaction parameter ϕ is simply assumed equals 1 (ϕ=1).

Surface tension of PLA Γ_{PLA}

The surface tension of PLA $\Gamma_{PLA} = 37.5$ mN m^{-1} was calculated from the Parachor P_s introduced by Quayle[43]

$$\Gamma_{PLA} = \left(\frac{P_{s,PLA}}{V}\right)^4 \qquad (A.2)$$

where $V = M/\rho$ is the molar volume of PLA, in which $\rho_{PLA} = 1.24$ g cm^{-3} and $M = 72.06$ are the mass density and the molar mass of PLA, respectively. The molar Parachor of PLA $P_{s,PLA} = 143.8$ was determined from the group contributions which are given in Table A.I.

Surface Tension of PVA Γ_{PVA}

It should be noted that the used PVA in this study is the partially PVA hydrolyzed 88% was prepared by the saponification of poly(vinyl acetate) (PVAc) having vinyl alcohol and vinyl acetate groups. This means that the chemical structure of PVA includes both the hydroxyl groups (—OH) and carbonyl (—$OCOCH_3$), as shown in Figure A.1, called poly(vinyl alcohol-*co*-vinyl acetate). The PVA hydrolyzed 88% means that poly(vinyl alcohol-*co*-vinyl acetate) has 88% mole percent of pure poly(vinyl alcohol) [—CH(OH)—CH2)—]$_m$ (PVOH) and 12% mole percent of pure poly(vinyl acetate) [—CH2—CH(OCOCH3)—]$_n$ (PVAc).

Table A.I. Atomic and Structural Contributions to the Parachor P_s Assigned by Quayle[44]

Unit	C	H	CH_2	O	O_2 (in esters)
Values assigned by Quayle	9.0	15.5	40.0	19.8	54.8

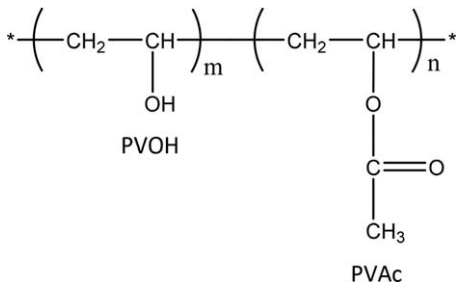

Figure A.1. Chemical structures of poly (vinyl alcohol-*co*-vinyl acetate).

Table A.II. Volume Percent of PVOH and PVAc in 1 Mole PVA

	Mass density (g cm^{-3})	Molar mass (g mol^{-1})	Molar volume (cm^3 mol^{-1})	% Volume
PVOH	1.26	44.2	35.08	32.66
PVAc	1.19	88.06	72.34	67.34

Like the calculation of the PLA surface tension Γ_{PLA}, the surface tension of PVOH Γ_{PVOH} and PVAc Γ_{PVAc} have values of 59 and 40 mN m^{-1}, respectively.[44]

Table A.II summarizes the calculation of volume percent of PVOH and PVAc for 1 mole PVA. In 1 mole PVA has 32.7% volume PVOH and 67.3% mole PVAc. If 1 mole PVA includes 88% mole PVOH and 12% PVAc, it has 78% volume PVOH and 22% volume PVAc.

Then, the surface tension of PVA Γ_{PVA} can be calculated as follows:

$$\Gamma_{PVA} = \Gamma_{PVOH} \times \text{vol \% PVOH} + \Gamma_{PVAc} \times \text{vol \% PVAc} \qquad (A.3)$$

$$\Gamma_{PVA} = \Gamma_{PVOH} \times 78\% + \Gamma_{PVAc} \times 22\% = 54.8 \qquad (A.4)$$

Using the eq. (A.1) with $\Gamma_{PLA} = 37.5$ mN m^{-1}, $\Gamma_{PVA} = 54.8$ mN m^{-1}, and ϕ=1, the interfacial tension between PLA and PVA is now 1.64 mN m^{-1}.

REFERENCES

1. Han, C. D.; Kim, Y. W. *Trans. Soc. Rheol.* **1975**, *19*, 245.
2. Tsebrenko, M. V.; Yudin, A. V.; Ablazova, T. I.; Vinogradov, G. V. *Polymer* **1976**, *17*, 831.
3. Vinogradov, G. V.; Krasnikova, N. P.; Dreval, V. E.; Kotova, E. V.; Plotnikova, E. P.; Pelzbauer, Z. *Int. J. Polym. Mater.* **1982**, *9*, 187.

4. Tsebrenko, M. V. *Int. J. Polym. Mater.* **1983**, *10*, 83.
5. Dreval, V. E.; Vinogradov, G. V.; Plotnikova, E. P.; Zabugina, M. P.; Krasnikova, N. P.; Kotova, E. V.; Pelzbauer, Z. *Rheol. Acta* **1983**, *22*, 102.
6. Min, K.; White, J. L.; Fellers, J. F. *Polym. Eng. Sci.* **1984**, *24*, 1327.
7. La Mantia, F. P.; Valenza, A.; Paci, M.; Magagnini, P. L. *Polym. Eng. Sci.* **1990**, *30*, 7.
8. Favis, B. D.; Therrien, D. *Polymer* **1991**, *32*, 1474.
9. Bordereau, V.; Carrega, M.; Shi, Z. H.; Utracki, L. A.; Sammut, P. *Polym. Eng. Sci.* **1992**, *32*, 1846.
10. Gonzalez-Nunez, R.; Favis, B. D.; Carreau, P. J.; Lavallée, C. *Polym. Eng. Sci.* **1993**, *33*, 851.
11. Chapleau, N.; Favis, B. D. *J. Mater. Sci.* **1995**, *30*, 142.
12. Lee, J. K.; Han, C. D. *Polymer* **2000**, *41*, 1799.
13. Covas, J. A.; Carneiro, O. S.; Maia, J. M. *Int. J. Polym. Mater.* **2001**, *50*, 445.
14. Pesneau, I.; Kadi, A. A.; Bousmina, M.; Cassagnau, P.; Michel, A. *Polym. Eng. Sci.* **2002**, *42*, 1990.
15. Filipe, S.; Cidade, M. T.; Wilhelm, M.; Maia, J. M. *Polymer* **2004**, *45*, 2367.
16. Wang, D.; Sun, G.; Chiou, B. S. *Macromol. Mater. Eng.* **2008**, *293*, 657.
17. Padsalgikar, A. D.; Ellison, M. S. *Polym. Eng. Sci.* **1997**, *37*, 994.
18. Yang, J.; White, J. L.; Jiang, Q. *Polym. Eng. Sci.* **2010**, *50*, 1969.
19. Tavanaie, M. A.; Shoushtari, A. M.; Goharpey, F.; Mojtahedi, M. R. *Fiber Polym.* **2013**, *14*, 396.
20. Tran, N. H. A.; Brünig, H.; Boldt, R.; Heinrich, G. *Polymer* **2014**, *55*, 6354.
21. Tran, N. H. A.; Brünig, H.; Heinrich, G. *J. Appl. Polym. Sci.* **2016**, DOI: 10.1002/app.44258
22. González-Núnez, R.; De Kee, D.; Favis, B. D. *Polymer* **1996**, *37*, 4689.
23. Merkus, H. K. In Particle Size Measurements; Merkus, H. K., Ed.; Springer: Netherlands, **2009**.
24. Blott, S. J.; Pye, K. *Sedimentology* **2008**, *55*, 31.
25. Harrats, C. In Multiphase Polymer-Based Materials: An Atlas of Phase Morphology at the Nano and Micro Scale; Harrats, C., Ed.; CRC Press: Boca Raton, FL, **2009**.
26. Favis, B. D.; Chalifoux, J. P. *Polymer* **1988**, *29*, 1761.
27. Bourry, D.; Favis, B. D. *Polymer* **1998**, *39*, 1851.
28. Heindl, M.; Sommer, M. K.; Münstedt, H. *Rheol. Acta* **2005**, *44*, 55.
29. Fakirov, S. *Compos. Sci. Technol.* **2013**, *89*, 211.
30. Taylor, G. I. *Proc. R. Soc.* **1932**, *138*, 41.
31. Wu, S. *Polym. Eng. Sci.* **1987**, *27*, 335.
32. Tran, N. H. A.; Brünig, H.; Hinüber, C.; Heinrich, G. *Macromol. Mater. Eng.* **2014**, *299*, 219.
33. Suparno, M.; Dolan, K. D.; Ng, P. K. W.; Steffe, J. F. *J. Food Process. Eng.* **2011**, *34*, 961.
34. Burkhardt, K.; Herrmann, H.; Jakopin, S. SPE ANTEC Tech. Pap. **1978**, *36*, 498.
35. Favis, B. D. In Polymer Blends: Formulation and Performance, Performance; Paul, D. R.; Bucknall, C. B., Eds.; Wiley: New York, **2000**.
36. Sundararaj, U.; Macosko, C. W. *Macromolecules* **1995**, *28*, 2647.
37. Roland, C. M.; Böhm, G. G. A. *J. Polym. Sci. Polym. Phys. Ed.* **1984**, *22*, 79.
38. Plochocki, A. P.; Dagli, S. S.; Andrews, R. D. *Polym. Eng. Sci.* **1990**, *30*, 741.
39. Favis, B. D.; Chalifoux, J. P. *Polym. Eng. Sci.* **1987**, *27*, 1591.
40. Allan, R. S.; Mason, S. G. *J. Colloid Sci.* **1962**, *17*, 383.
41. Taylor, G. I. *Proc. R. Soc.* **1934**, *146*, 501.
42. Girifalco, L. A.; Good, R. J. *J. Phys. Chem.* **1957**, *61*, 904.
43. Quayle, O. R. *Chem. Rev.* **1953**, *53*, 439.
44. Van Krevelen, D. W.; Nijenhuis, K. T. In Properties of Polymers; Van Krevelen, D. W.; Nijenhuis, K. T., Eds.; Elsevier: Amsterdam, **2009**.